^{113}Cd NMR study of transferred hyperfine interactions in the dilute magnetic semiconductors $Cd_{1-x}Co_xS$ and $Cd_{1-x}Fe_xS$ and impurity distribution in $Cd_{0.994}Co_{0.006}S$

V. Ladizhansky, V. Lyahovitskaya, and S. Vega
Department of Chemical Physics, Weizmann Institute of Science, 76100 Rehovot, Israel
(Received 5 March 1999)

Diluted magnetic semiconductor samples $Cd_{0.99}Fe_{0.01}S$ and $Cd_{0.994}Co_{0.006}S$ were investigated by ^{113}Cd magic angle spinning NMR spectroscopy in the temperature range of 180–400 K. These alloys were prepared by mixing $Cd_{0.97}M_{0.03}S$ ($M=$Co, Fe) and the binary compound CdS in the appropriate molar ratios and maintaining the mixtures at about 1000 °C for seven days. The macroscopic homogeneity of the samples was determined by energy dispersive spectroscopy. The microscopic homogeneity of the paramagnetic ion distribution in these samples can be studied by analyzing their ^{113}Cd NMR spectra. These spectra contain a set of Cd* bands (the * sign indicates the observed cadmium atoms) that are shifted by the transferred hyperfine (THF) interaction between the cadmium nuclei and their neighboring paramagnetic ions. Using the temperature dependence of the positions, the relaxation times, and anisotropies of these bands, we assigned each band to a well-defined next-nearest neighbor $M(2)$-S-Cd(1)-S-Cd* conformation, and correlated the THF interaction constants of all conformations to the $M(2)$-Cd* distances. All cadmium bands in the spectra comprise a set of lines that correspond to Cd* atoms in conformations of the type $M(3)$-S-Cd(2)-S-Cd(1)-Cd*-S-Cd(1)-S-$M(2)$. The relative intensities of the lines can be calculated for given x values, when we assume a random magnetic ion impurity distribution. For the $Cd_{0.994}Co_{0.006}S$ sample, we found that the calculated line intensities were not consistent with the experimental intensities. To explain this deviation and to simulate a spectrum that fits the experimental data, we assumed that this sample consists of clusters with different concentrations of the impurity. Good agreement was obtained when about half of the cadmium atoms do not interact with the paramagnetic ions, and the other half interacts with ions that are randomly distributed in an alloy composed of $Cd_{0.987}Co_{0.013}S$. [S0163-1829(99)14335-2]

I. INTRODUCTION

In recent years, bulk diluted magnetic semiconductors (DMS),[1–4] and especially their low-dimensional structures, have received considerable attention.[5–8] The lattice constants and band parameters of these alloys depend strongly on the concentration of the paramagnetic ions. Also, their magnetic properties are substantially modified in the presence of magnetic impurities.[2–4,9–12] These properties result from long-range exchange (superexchange) interactions that are mediated by the spin polarization of the electron-density distributions between the paramagnetic ions. Moreover, the magnitudes of these interactions are strongly dependent on bond lengths and angles, as well as on the covalence strengths and orbital hybridization of the bonds connecting the paramagnetic impurities.[13,14]

Another type of interaction that occurs in DMS alloys is the transferred hyperfine (THF) interaction between the unpaired electrons of the paramagnetic ions and the nuclear spins of nonmagnetic atoms. The transfer of the electron-spin polarization takes place via electronic orbitals, and is similar to that of the superexchange interaction. Hence, a better understanding of how the THF interaction is correlated with the bond properties of the interacting atoms can provide information about the electronic mechanism of the superexchange interaction. Nuclear spins provide natural probes for detecting local magnetic properties. ^{113}Cd NMR was used to investigate THF interactions in the alloys $Cd_{1-x}Mn_xTe$ (Ref. 15) and $Cd_{1-x}Fe_xTe$,[16] with a zinc-blende structure, as well as in $Cd_{1-x}Mn_xSe$, $Cd_{1-x}Fe_xSe$, and $Cd_{1-x}Co_xSe$,[17] having a wurtzite structure. The different lines in the ^{113}Cd NMR spectra of these samples were assigned to different cadmium atoms, which experience distinct THF interactions. We were able to differentiate between ^{113}Cd* atoms in different next-nearest-neighbor (2N) conformations, $M(2)$-A-Cd(1)-A-Cd*, with $M=$Mn, Fe, Co and $A=$Te, Se, where the asterisk indicates the cadmium atoms that correspond to certain lines in the spectra.

Here we report on the results of a ^{113}Cd NMR study of the wurtzite $Cd_{1-x}Fe_xS$ and $Cd_{1-x}Co_xS$ alloys,[3] and show that the NMR results can be used to determine the microscopic homogeneity of these DMS samples. In the wurtzite structure one can identify 44 types of 2N cadmium atoms, which can be divided into 11 conformations. Each conformation is characterized by four bonds, $M(2)$-A-Cd(1)-A-Cd*, and can be defined by the dihedral angles of the third and fourth bond starting from $M(2)$-A[17], with M replacing a cadmium site in the crystal. In Table I the 11 2N conformations in the wurtzite structure are defined and numbered from I to XI, and the atomic distances $M(2)$-Cd* are given for $Cd_{1-x}M_xS$. In some of the configurations, two or four bond pathways are present simultaneously. The 11 types of cadmiums can result in a maximum of 11 THF-shifted ^{113}Cd NMR lines with intensities determined by the number of sites in each conformational set. Different conformations may result in the same hyperfine constants. For $Cd_{1-x}Fe_xSe$ and $Cd_{1-x}Co_xSe$ alloys,[17] the comformational assignments were made by fitting the experimental relaxation times and

 ©1999 The American Physical Society

TABLE I. Bond conformations, number of sites, and distances between the paramagnetic ions (M) and the cadmium atoms of the 11 sets of 2N cation configurations in the wurtzite lattice. In addition, the number of sites and the range of distances are given for 3N(+) and 4N(+) conformations.

Notation	2N conformations in CdMS	Number of sites	Distance, Å
I	(180°,180°)	6	8.25
II	(120°,180°)	6	7.87
III	(180°,120°)	6	7.87
IV	(180°,60°)+(180°,−60°)	3	7.2
V	(−60°,180°)+(60°,180°)	3	7.2
VI	(−60°,180°)+(−60°,−120°)	6	7.2
VII	(180°,−60°)+(−120°,−60°)	6	7.2
VIII	(180°,0°)	1	6.7
IX	(0°,180°)	1	6.7
X	(60°,60°)+(−60°,−60°)	3	5.85
XI	(−120°,60°)+(60°,60°)+(−60°,−60°)+(120°,−60°)	3	5.85
3N(+)		96	9.2–12.58
4N(+)		170	13.04–16.5

intensities of the lines to theoretical values.

^{113}Cd* atoms surrounded by two paramagnetic ions, one in a 2N conformation and one in a 3N conformation, M(3)-S-Cd(2)-S-Cd(1)-S-Cd*, will experience different hyperfine shifts. The influence of these conformations on the spectra is negligible for low concentrations with $x<0.004$, but should be taken into account for higher concentrations. For example, in wurtzite crystals, the probability of finding a Cd atom with only one 2N paramagnetic neighbor, and a Cd atom with one neighbor in a 2N site and one or two neighbors in 3N sites becomes equal when $x=0.008$. For higher x values the latter conformation dominates and its corresponding NMR lines will have higher intensities than those of the 2N conformation. This was not taken into account when the ^{113}Cd spectra of DMS alloys were previously analyzed, but will be investigated here.

In the following sections we will discuss the magic angle spinning (MAS) ^{113}Cd NMR experiments on the sulfur-based alloys $Cd_{0.99}Fe_{0.01}S$ and $Cd_{0.994}Co_{0.006}S$, conducted at various temperatures and spinning speeds. Section II describes the sample preparation procedure and gives the parameters of the NMR experiments. In Sec. III we present the ^{113}Cd MAS NMR spectra of the $Cd_{1-x}M_xS$ samples and the derivation of THF coupling constants of the lines in the spectra and their conformational assignments. In Sec. IV we analyze the existing fine structure of the lines by taking into account THF shifts caused by 3N paramagnetic ions. For the $Cd_{0.994}Co_{0.006}S$ sample all possible 3N conformations were considered and combined with the 2N conformations to calculate a spectrum based on a random distribution of the paramagnetic ions. The descrepancies between this spectrum and the experimental one can be explained by assuming a microscopic inhomogeneity of the paramagnetic ion distribution in the sample. In the final discussion we compare THF interaction constants from selenium- and sulfur-based $Cd_{1-x}M_xA$ alloys, showing the similarity between their line assignments to 2N conformations and their M(2)-Cd* distance dependence.

II. EXPERIMENT

A. NMR measurements

The NMR experiments were done using a home-built 200-MHz NMR spectrometer and a Bruker 300-MHz CXP NMR spectrometer. The Larmor frequencies of ^{113}Cd in these spectrometers are 44.37 and 66.55 MHz, respectively. All measurements were done on samples rotating in the external magnetic field at the magic angle. High-speed 5- and 7-mm MAS probes from Doty Scientific, Inc., and a 4-mm Bruker MAS probe were used for the experiments on the 200- and 300-MHz spectrometers, respectively. The temperature studies were done at 300 MHz, and a Bruker Variable-Temperature-Unit W110512 was used for sample cooling and heating with a temperature stability of ±0.2 K. The spinning frequencies of the samples varied between 1.5 and 7.5 kHz and had a stability of 30 Hz or less.

The spin-echo sequence $\{\pi/2-\tau-\pi-\tau-(\text{acquisition})\}$ was used for detecting the signals in all the experiments. The length of the $\pi/2$ pulse varied from 3.5 to 4 μs, and the delay time τ was always equal to the length of one rotor period. Spin-lattice relaxation times of ^{113}Cd nuclei were measured using the saturation recovery sequence $\{(\pi/2-t)_n-T-\pi/2-\tau-\pi-\tau-(\text{acquisition})\}$ with $n>20$. In these experiments the amplitudes of the lines in the Fourier-transformed spectra were monitored as a function of T, and fitted to single exponents.

B. Sample preparation

Polycrystalline samples of $Cd_{1-x}Co_xS$ and $Cd_{1-x}Fe_xS$ were prepared with x values of 0.006 and 0.01, respectively. A two-stage preparation procedure was used to overcome the inaccuracy of weighing small amounts of initial compounds.

At the first stage, the CoS and FeS binary compounds were synthesized by direct fusion of a mixture of 5N pure elements in a molar ratio of 1:1.1, and subsequently evacuation of the mixture in quartz ampoules to 10^{-5} Torr. The sealed ampoules were then heated at a rate of 50 °C/h up to

800 °C, and kept at that temperature for four days, after which that they were annealed at 900 °C. The resulting FeS and CoS compounds were mixed with CdS in molar ratios of 97:3 to produce $Cd_{0.97}Fe_{0.03}S$ and $Cd_{0.97}Co_{0.03}S$, then thoroughly milled in an agate mortar and finally loaded into carbon-coated quartz ampoules. The next preparation procedure was as follows: (i) the mixture was kept at 200 °C for 1 h in a constant flow of $H_2S+N_2+H_2$ to remove residual water; (ii) the ampoules were then sealed in a vacuum of 10^{-5} Torr and sintered at 500–600 °C for two days, then the temperature was raised to 800 °C and the ampoules were kept at that temperature for another two days; (iii) the temperature was increased to 900–1000 °C and the samples were annealed for seven days, and (iv) the sintered polycrystalline ingots were milled and annealed at 900 °C for ten days for a second time in order to improve the homogeneity of the distribution of impurities.

The resulting compounds with $x=0.03$ were then used to prepare $Cd_{1-x}Co_xS$ and $Cd_{1-x}Fe_xS$ for $x=0.006$ and 0.01, respectively. They were again mixed with pure CdS in appropriate molar ratios, thoroughly milled in an agate mortar and loaded into carbon-coated quartz ampoules. Steps (i)–(iv) were then repeated.

All samples were characterized by energy Dispersive (X-ray fluorescence) Spectroscopy (EDS). In our experiments we used only samples that were single-phase compounds with macroscopic homogeneously distributed magnetic ions. The measured concentrations were in good agreement with those expected from the preparatory procedure, with a variation of less than 5%.

III. NMR RESULTS

A. Spectral line positions

Figure 1 shows representative ^{113}Cd spectra obtained from $Cd_{0.994}Co_{0.006}S$ and $Cd_{0.99}Fe_{0.01}S$. The overall shape of these spectra is very similar to those of the $Cd_{1-x}Co_xSe$ and $Cd_{1-x}Fe_xSe$ samples,[17] and can be interpreted similarly. The lines at 0 ppm correspond to the ^{113}Cd line position of the bulk binary compound CdS. All additional lines shift linearly with inverse temperature, indicating that they originate from the THF interaction between the cadmium nuclei and the paramagnetic ions. All of the frequency bands show fine structures that can be decomposed into a set of lines. The spread of these lines in each band is about 20 ppm. For determining the conformational assignments, the NMR parameters of the strongest lines of each band were measured. At the high-temperature limit ($B_0/T \ll 1$) the temperature dependence of the shifts closely follows the Curie-Weiss law

$$\Delta\nu_i = \left[\frac{A}{h}\right]_i \frac{g\beta S(S+1)B_0}{3k_BT} + \Delta\nu_{0i}, \qquad (1)$$

where $\Delta\nu_i$ is the shift of the ith line from the bulk line at 0 ppm, B_0 is the external magnetic field, equal to 7.05 T for the 300-MHz spectrometer, $\Delta\nu_{0i}$ is the temperature-independent contribution from the chemical shift interaction, and $[A/h]_i$ is the strength of the hyperfine interaction of the nuclei in the ith group with the paramagnetic ion. The values of the hyperfine constants were extracted from the slope of $\Delta\nu_i(1/T)$ for the largest peak in each band. They were derived using g values of 2.3 for $Cd_{1-x}Co_xS$ and $Cd_{1-x}Fe_xS$.[18] The g value for the $Cd_{1-x}Fe_xS$ sample was not known to us, so we assumed that it equals the value of the Co^{+2} alloys. This is justified by realizing that the g factors of $Cd_{1-x}Fe_xSe$ and $Cd_{1-x}Co_xSe$, $g=2.29$ (Ref. 11) and $g=2.30$,[19] respectively, are almost equal. The S values are 1.5 for Co^{2+} and 2 for Fe^{2+}. Table II summarizes the THF interaction constants for the different lines as well as the temperature-independent chemical shift contributions. Because of the widths of the frequency bands, the tabulated values may deviate from their actual values by about 10%. In addition, the values of the isotropic chemical shifts of the different lines are larger than those in the selenium-based alloys. The absolute values of these shifts increase with increasing THF constants.

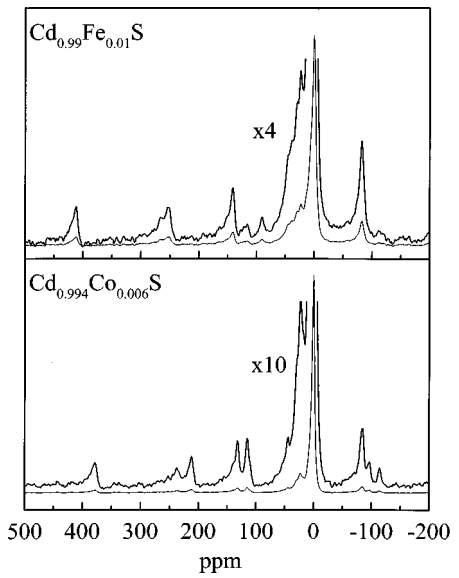

FIG. 1. ^{113}Cd MAS NMR spectra of the $Cd_{0.99}Fe_{0.01}S$ and $Cd_{0.994}Co_{0.006}S$ alloys. The spectra were obtained by Fourier transformation of the echo signals at a spinning speed of 5.2 kHz after 3600 scans. The delay time between accumulations was 10 sec. The ppm scale was chosen with respect to pure CdS. The low-intensity features of the spectra are emphasized by multiplying the spectra by factors indicated in the figure. The spectrum of the $Cd_{0.994}Co_{0.006}S$ is a fully T_1 relaxed spectrum, whereas the $Cd_{0.99}Fe_{0.01}S$ spectrum is not. ($T_1 > 10$ sec).

B. Anisotropic contributions

To check the assignment of the spectral lines to the 2N configurations, we measured the anisotropic contributions to the line shifts of the powder samples by monitoring their MAS sideband intensities, as was done for the selenium alloys.[17] The sideband patterns were obtained for different spinning speeds and at different temperatures at a magnetic field of 7.05 T. Both the dipolar and THF interactions contribute to the magnitude of these anisotropies. The anisotropic part of the THF interaction is usually much smaller than the contribution $\Delta^i\nu_{\mathrm{dip}}$ of the dipolar interaction between observed ^{113}Cd* nuclei and the effective magnetic moment of their nearest-neighboring paramagnetic ions.[20] Hence the experimental values of the temperature-dependent anisotropies are about equal to the dipolar contributions.

TABLE II. The THF interaction constants of the lines at positions $\Delta\nu$ at ambient temperature, together with the temperature-independent isotropic chemical shift values $\Delta\nu_0$ in the cadmium alloys $Cd_{0.99}Fe_{0.01}S$ and $Cd_{0.994}Co_{0.006}S$.

	$Cd_{1-x}Fe_xS$			$Cd_{1-x}Co_xS$	
$\Delta\nu$, ppm	$\frac{A}{h}$, MHz	$\Delta\nu_0$, ppm	$\Delta\nu$, ppm	$\frac{A}{h}$, MHz	$\Delta\nu_0$, ppm
412	0.709	−231	378	1.03	−209
267	0.454	−145	237	0.642	−133
253	0.407	−115	212	0.486	−118
141	0.239	−76	132	0.312	−80
90	0.160	−58	114	0.254	−61
38	0.106	59	22	0.046	−11
−82	−0.145	49	−84	−0.215	60

These contributions are temperature dependent, following the temperature dependence of the effective magnetic moment $\langle\mu\rangle$ of the ion:

$$\Delta\nu^i_{dip}=\frac{1}{r_i^3}\gamma_N\langle\mu\rangle=\frac{(g\beta)^2\gamma_N S(S+1)}{3r_i^3k_BT}B_0, \qquad (2)$$

where r_i is the distance between the magnetic ion and the ith cadmium. These contributions can be calculated for known r_i values. For example, the dipolar anisotropy of a 1N cadmium nucleus $^{113}Cd^*$ interacting with a $Co^{2+}(1)$ ion at a distance $r_{1N}=4.12$ Å is 13 kHz at room temperature (in a field of 7.05 T), and 16.7 kHz at $T=240$ K, and varies between 1.6 and 4.6 kHz for 2N·Co(2)-$^{113}Cd^*$ pairs with $r_{2N}=5.85-8.25$ Å at room temperature. The measurements of the sideband intensities of the lines in the spectra are complicated by the overlap of the sideband patterns of the different lines and the poor signal-to-noise ratios of the spectra at low spinning speeds (1.5–3.0 kHz). This made it difficult to analyze the MAS patterns accurately. However, we were able to estimate the anisotropic contributions for part of the lines of the $Cd_{0.994}Co_{0.006}S$ sample with an accuracy of 1 kHz, using the Herzfeld-Berger[21] analysis of the relative sideband-to-centerband intensity ratios. These anisotropies vary from 3.9 to 4.9 kHz at room temperature and from 5.2 to 6.4 kHz at $T=240$ K. The values are substantially smaller than the expected anisotropy of the nearest-neighboring 1N configuration, and are of the order of the magnitudes of the

TABLE III. Spin-lattice relaxation times of the ^{113}Cd lines in $Cd_{0.994}Co_{0.006}S$ and in $Cd_{0.99}Fe_{0.01}S$, and the assignment of these lines to the I–XI 2N conformations and the 3N(+) conformations based on the overall agreement between the theoretical and experimental T_1 values of the conformations.

		$Cd_{0.994}Co_{0.006}S$		
$\Delta\nu$, ppm	T_1, msec (experimental)	Assignment	Total number of sites	T_1, msec (theoretical)
378	102±7	X+XI	6	102
237	206±36	VIII+IX	2	230
212	304±17	VII	6	354
132	380±40	V+VI	9	354
114	819±36	I+IV	9	354,801
22	969±20	3N+	96	>1000
−84	410±34	II+III	12	604
		$Cd_{0.99}Fe_{0.01}S$		
$\Delta\nu$, ppm	T_1, msec (experimental)	Assignment	Total number of sites	T_1, msec (theoretical)
412	198±18	X+XI	6	198
267	460±71	VIII+IX	2	451
253	559±36	VII	6	683
141	910±23	V+VI	9	683
114	[a]	I	3	683
90	1237±234	IV	6	1555
38	5000±56	3N+	96	>2000
−82	930±20	II+III	12	1169

[a]Could not be determined because of a low S/N ratio.

interaction expected from next-nearest M^{+2} neighbors. This indicates that the observed lines correspond mainly to the 2N configurations, similar to the results of $Cd_{1-x}Co_xSe$.[17]

C. T_1 relaxation time measurements

In the case of the selenium alloys the assignment of the lines to the 2N configurations was mainly based on the values of their T_1 relaxation times, and to a lesser extent on the analysis of the relative intensities of the lines. Here this was again possible, and in Table III the theoretical and experimental T_1 values are compared and their assignments presented. When the relaxation parameters are dominated by interactions with the paramagnetic impurities, the spin-lattice relaxation rates have two contributions[22,23]

$$\left[\frac{1}{T_1}\right]_i = \frac{2}{15}S(S+1)g^2\mu_B^2\gamma_I^2\frac{1}{r_i^6}\left[\frac{3\tau}{1+(\omega_I\tau)^2}+\frac{7\tau}{1+(\omega_s\tau)^2}\right], \\ +\frac{3}{2}S(S+1)\left[\frac{A}{h}\right]_i^2\frac{\tau}{1+(\omega_s\tau)^2}, \quad (3)$$

where the first term is due to fluctuations in the dipolar interaction between the magnetic moment of a paramagnetic ion and a neighboring nuclear cadmium spin, and the second term is due to the THF interaction. The value γ_I is the nuclear magnetogyric ratio, r_i is again the distance between the paramagnetic ion and a Cd* in the ith configuration, τ is the electron-spin-lattice relaxation time of the paramagnetic ion, ω_s is the electronic Larmor frequency, and ω_I is the nuclear Larmor frequency. As was shown previously for $Cd_{1-x}Co_xSe$ and $Cd_{1-x}Fe_xSe$,[17] the first term in Eq. (3) controls the spin-lattice relaxation rates.

T_1 values were measured by conducting saturation recovery experiments. Assuming that the line at 378 ppm with the shortest relaxation time belongs to the 2N cadmium with the closest possible distance $r_i = 5.85$ Å, one obtains, by using Eq. (3), a value for the electronic correlation time τ that is about 1.3×10^{-11} sec. All other T_1 values of the various 2N configurations can then be estimated by inserting this τ value in Eq. (3) and using the r_i values listed in Table I. The experimental as well as calculated values for the T_1 relaxation times are tabulated in Table III, together with the result of the line assignment. Note that the line at 114 ppm, corresponding both to the I and IV configurations with respective r-values of 8.25 and 7.2 Å, should have a biexponential relaxation behavior as indicated in the table. This was not observed because of low signal-to-noise (S/N) ratio values, and only the largest T_1 was obtained.

IV. PARAMAGNETIC ION DISTRIBUTION IN $Cd_{0.994}Co_{0.006}S$

As mentioned, the spectral assignments of the ^{113}Cd lines in the spectra of $Cd_{1-x}M_xS$, as well as of $Cd_{1-x}M_xSe$,[17] to the different 2N atomic conformations were mainly based on their anisotropies and relaxation times, and to a lesser extent on the integrated line intensities. Because all frequency bands in the spectra are composed of a set of lines, spread over a range of about 20 ppm, as can be seen in Fig. 2 for $Cd_{0.994}Co_{0.006}S$, line-shape analysis must take into account

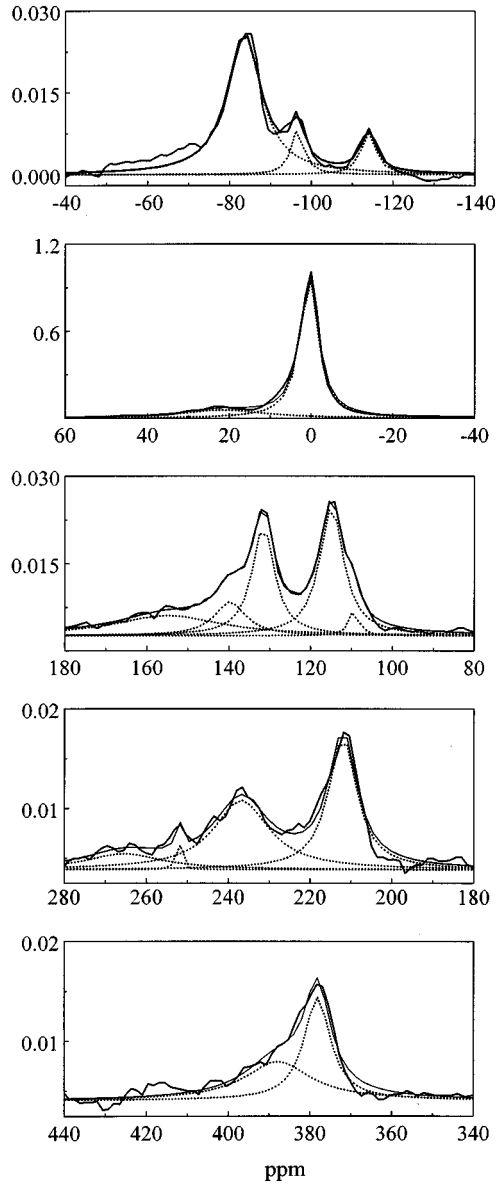

FIG. 2. Multi-Lorentzian line fitting of the spectral bands in the ^{113}Cd spectrum of $Cd_{0.994}Co_{0.006}S$, shown in Fig. 1. The intensity of the lines at 0 ppm was chosen to be unity, and the other lines are normalized accordingly. The dotted lines represent the Lorentzian curves. The thin solid lines are the sum of the individual Lorentzians, and the thick solid lines are the experimental spectra.

THF interactions with paramagnetic ions in the 3N and 4N conformations. In Fig. 2 the six distinct spectral bands between -140 and 440 ppm of the $Cd_{0.994}Co_{0.006}S$ sample are drawn separately and decomposed into a set of Lorenzian lines at different frequencies and with different linewidths. Since the cadmium nuclei with magnetic ions in the $M(1)$-S-Cd* configuration cannot be observed because of their short relaxation times, and two M^{+2} ions in two 2N conformations of the same nucleus shift and broaden their lines appreciably, we concluded that the shifted lines in the spectral bands are due to nuclei with one 2N magnetic ion and no additional 3N ion or to nuclei with one 2N ion and at least one 3N ion $M(3)$-S-Cd(2)-S-Cd(1)-S-Cd*-S-Cd(1)-S-$M(2)$ in their (2N+3N) conformations. The lines close to 0 ppm correspond to cadmium atoms with no paramagnetic

TABLE IV. Calculated occupational probabilities of the distinguishable configurations of $Cd_{0.994}Co_{0.006}S$ (I) and of [47%$Cd_{0.987}Co_{0.013}S$+53%CdS] (II), together with their experimental line intensities and positions in the spectrum. The asterisks indicate values that cannot be distinguished experimentally.

Conformation		Calculated intensities of I	Calculated intensities of II	Experimental intensities	Assignment (shift, ppm)
I+IV	2N	0.054	0.016	0.010	140
	2N+3N(1,2)	0.038	0.031	0.028	114
II+III	2N	0.72	0.021	0.015	−114
	2N+3N(1,2)	0.05	0.044	0.045	−84
	2N+3N(3+)	0.003	0.009	0.006	−97
V+VI	2N	0.054	0.016	0.019	154
	2N+3N(1,2)	0.038	0.031	0.023	132
VII	2N+2N(1,2)	0.036	0.021	0.019	212
	2N	0.025	0.011*	-	237
VIII+I	2N+3N(1,2)	0.012	0.007*	0.019	237
X	2N	0.008	0.004	0.006	265
X+XI	2N	0.036	0.011	0.010	395
	2N+3N(1,2)	0.025	0.021	0.019	378
3N(+)	3N(+)	0.57	0.280	0.241	24
4N(+)	4N(+)	1	1	1	0

ions in the 44 sites of their 2N configurations, and at least one in one of the 96 sites of the 3N configurations. The line with the largest intensity close to 0 ppm is located at 21 ppm. The values of the integrated intensities of the individual lines are proportional to the occupational probabilities of these combined conformations. The integrated intensities of all Lorenzian lines in Fig. 2, normalized to an intensity of 1 for the line at 0 ppm, are tabulated in Table IV. The low-intensity lines at 45, 110, and 253 ppm have not been taken into account in our simulations. All pair configurations show two lines, with the exception of (II+III) with three lines. To analyze these values we calculated the probabilities $P_i(x,n_i,N_i)$ of finding n_i neighbors among N_i sites in the ith conformation for a given concentration x of the paramagnetic ions

$$P_i(x,n_i,N_i)=C_{n_i}^{N_i}x^{n_i}(1-x)^{N_i-n_i}$$

$$=\frac{N_i!}{n_i!(N_i-n_i)!}x^{n_i}(1-x)^{N_i-n_i}, \qquad (4)$$

as well as the probabilities of finding n_1 ions in one conformation 1 with N_1 sites and at the same time n_2 in another conformation 2 with N_2 sites,

$$P_{i_1\cdot i_2}(x,n_1,N_1;n_2,N_2)=P_{i_1}(x,n_1,N_1)P_{i_2}(x,n_2,N_2). \qquad (5)$$

Assuming a random distribution of the paramagnetic ions in the cobalt alloy with $x=0.006$, a set of probabilities was obtained for all single and pair configurations (II+III), (I+IV), (VIII+IX), (VII), (X+XI) as follows. For 2N, one ion in a 2N configuration and no ion in a 3N configuration; for 2N+3N(1,2), one ion in a 2N configuration and one or two ions in a 3N configuration; and 2N+3N(3+), one ion in a 2N configuration and at least three ions in a 3N configuration. For the unoccupied 2N conformations, we have, for 3N(+), at least one ion in a 3N configuration and no ion in the 2N configurations, and for 4N(+), at least one ion in a 4N configuration and no ion in the 2N or 3N configurations. These probabilities were normalized in such a way that the probability of 4N(+), corresponding to the main line in the spectrum, was 1. The number of ion neighbors in 4N configurations is 170 for the wurtzite structure. This value, together with the 96 3N neighbors, was used for calculating the occupational probabilities for 4N(+), 3N(+), and 2N+3N configurations. The results of this calculation are summarized in Table IV and the corresponding band structures of the spectra, are shown in Fig. 3. In these simulated spectra the experimental line positions and widths were used together with theoretical line intensities derived from the probabilities. Clearly, there is no agreement between the experimental and calculated intensities. Therefore, a nonuniform random distribution of the paramagnetic ions must be used to fit the experimental data. Such a distribution was found by combining two types of crystal structures of $Cd_{1-x}Co_xS$, with randomly distributed Co^{+2} ions for two different x values, and mixing them at a microscopic level such that the macroscopic concentration of the ions in the sample still corresponds to $x=0.006$. To fit the experimental data, the following algorithm was used. Relative occupancies p_1 and p_2 and concentrations x_1 and x_2 were allowed to vary under the constrains $p_1+p_2=1$ and $p_1x_1+p_2x_2=0.006$. p_1 and x_1 were chosen, and p_2 and x_2 were calculated from the above formulas. p_1 and x_1 were allowed to vary until the best fit between experimental and calculated intensities was obtained. The best agreement was obtained by taking a mixture of 53% of the binary compound CdS with $x=0$ and 47% of the $Cd_{1-x}Co_xS$ alloy with $x=0.013$. The results for this mixture are summarized in Table IV, and the corresponding line shapes of the six spectral bands are shown in Fig. 3. This time a good agreement was reached with the experimental spectra. This binary mixture, however, is not necessarily the only macroscopic structure that results in a good fit with the experimental data and at the same time agrees with the EDS results, indicating that $x=0.006$. Our solution, therefore, in-

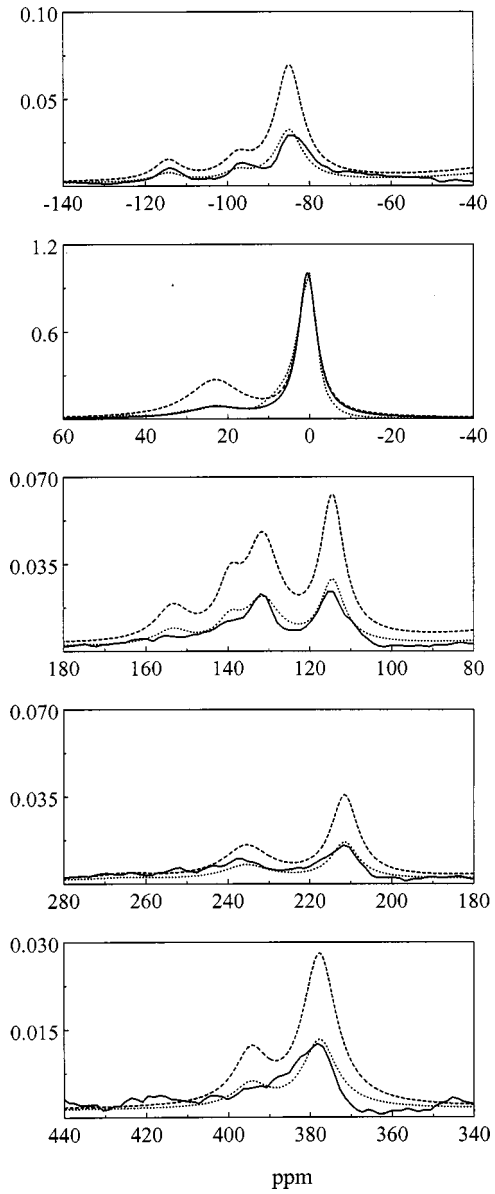

FIG. 3. Comparison of the simulated and experimental ^{113}Cd spectrum of $Cd_{0.994}Co_{0.006}S$. The solid lines are the experimental results, also shown in Figs. 1 and 2. The dashed lines are the calculated line shapes of $Cd_{0.994}Co_{0.006}S$ and the dotted lines are the calculated line shapes of a (53% CdS+47% $Cd_{0.987}Co_{0.013}S$) mixed sample.

dicated that the binary CdS compound is not uniformly doped by a random distribution of Co^{+2} ions with $x=0.006$, but that at some microscopic scale the cadmium atoms have paramagnetic environments corresponding to x values of 0–0.013.

A similar analysis of the Fe-based alloys was not possible because the Cd* relaxation times of the 3N(+) and 4N(+) conformations are too long to obtain a fully relaxed spectrum with a sufficient signal-to-noise ratio. However, the spectrum in Fig. 1 reveals that we obtain the same type of multiline structure as for the cobalt alloy, with slight changes around the lines at 90 ppm and a multiline structure of the 3N(+) spectrum.

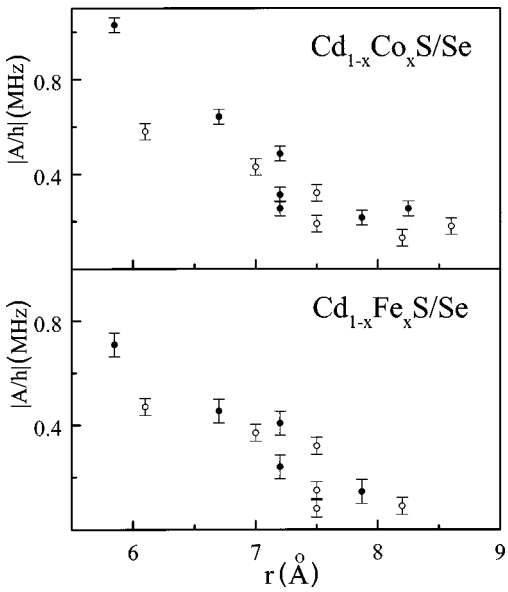

FIG. 4. The absolute values of the transferred hyperfine interaction constants of the 2N conformations $M(2)$-S-Cd(1)-S-Cd* plotted as a function of $M(2)$-Cd* distances for four compounds: the open circles are the constants of $Cd_{0.994}Co_{0.006}Se$ (upper graph) and $Cd_{0.99}Fe_{0.01}Se$ (lower graph), and the solid circles are the constants of $Cd_{0.994}Co_{0.006}S$ (upper graph) and $Cd_{0.99}Fe_{0.01}S$ (lower graph). The values of the transferred hyperfine constants of the Se-based compounds were taken from Ref. 17. The error bars indicate the uncertainties in the values of the THF constants that are a result of the frequency spreads of the 2N bands in the Cd spectra.

V. SUMMARY AND DISCUSSION

^{113}Cd NMR has been used to monitor long-range spin polarization transfer mechanisms in $Cd_{1-x}Co_xS$ and $Cd_{1-x}Fe_xS$ alloys. Specifically, we assigned the ^{113}Cd NMR lines to the specific next-nearest-neighbor conformations $M(2)$-S-Cd(1)-S-Cd* of the paramagnetic ions with a result very similar to that of $Cd_{1-x}Co_xSe$ and $Cd_{1-x}Fe_xSe$. When the results of Tables II and III are compared with the results of the selenium compounds, clearly the THF constants of the CdS-based alloys are larger than those of the CdSe-based alloys. Although both alloys show wurtzite structures, the difference must be attributed to the dissimilarity in their unit cell dimensions; the lattice parameters are $a=4.1348$ Å and $c=6.7490$ Å for CdS, and $a=4.3$ Å and $c=7.02$ Å for CdSe. Unfortunately, we do not have a simple model, based on the bond structures involved in the spin polarization transfer, which would enable us to calculate the THF parameters and explain why certain conformations result in negative interaction constants. However, it is interesting to compare these values for the four alloys $Cd_{1-x}M_xA$ with $M=$ Fe, Co and $A=$ Se, S. The THF interaction strengths and the efficiency of spin polarization transfer from the paramagnetic ion $M^{+2}(2)$ to the observed Cd* cation depend on the bond lengths and angles of the connecting structural configurations as well as on the type of intervening atoms. The direct distances between the $M^{+2}(2)$ and Cd* atoms depend on these parameters and on the dihedral angles given in Table I. It is not practical to represent the dependence of the THF constant on these dihedral angles, but we have noted that there is

a correlation between the THF constants and the direct $M(2)$-Cd* distances of the assigned 2N conformations. This correlation is shown in Fig. 4 for the four alloys. Surprisingly, there seems to be some linear dependence between the THF parameters and the through space distances. Conformations IV, V, VI, and VII have the same $M(2)$-Cd* distance, 7.2 Å for CdS, but show different THF values, indicating their dependence on dihedral angles. Conformation VII has the strongest hyperfine shift, and conformation IV the smallest among the four. These observations could be investigated theoretically to obtain a better understanding of the spin polarization in the DMS alloys.

ACKNOWLEDGMENT

This work was supported by the Minerva Foundation.

[1] *Semiconductors and Semimetals*, edited by J. K. Furdyna and J. Kossut (Academic, New York, 1988), Vol. 25.
[2] J. K. Furdyna, J. Appl. Phys. **64**, R29 (1988).
[3] W. J. M. de Jonge and H. J. M. Swagten, J. Magn. Magn. Mater. **100**, 322 (1991).
[4] A. Twardowski, Y. F. Chen, W. C. Clou, and M. Demianiuk, Solid State Commun. **90**, 493 (1994).
[5] S. Datta, J. K. Furdyna, and R. L. Gunshor, Superlatt. Microstruct. **1**, 294 (1985).
[6] A. Twardowski, Chin. J. Phys. **33**, 375 (1995).
[7] S. J. Weston, M. O'Neill, J. E. Nicholls, J. Miao, W. E. Hagston, and T. Stimmer, Phys. Rev. B **58**, 7040 (1998).
[8] Y. Oka, K. Yanata, H. Okamoto, M. Takahashi, and Jinxi Shen, Solid-State Electron. **42**, 1267 (1998).
[9] A. Mycielski, J. Appl. Phys. **63**, 3279 (1988).
[10] Y. Shapira, J. Appl. Phys. **67**, 5090 (1990).
[11] A. Lewicki, J. Spalek, and A. Mycielski, J. Phys. C **20**, 2005 (1987).
[12] S. P. McAlister, J. K. Furdyna, and W. Giriat, Phys. Rev. B **29**, 1310 (1984).
[13] J. Spalek, A. Lewicki, Z. Tarnawski, J. K. Furdyna, Z. Obszko, and R. R. Galazka, Phys. Rev. B **33**, 3407 (1988).
[14] A. Bruno and J. P. Lascaray, Phys. Rev. B **38**, 9168 (1988).
[15] K. Beshah, P. Becla, R. G. Griffin, and D. Zamir, Phys. Rev. B **48**, 2183 (1993).
[16] M. Gavish, S. Vega, and D. Zamir, Phys. Rev. B **48**, 2191 (1993).
[17] V. Ladizhansky, A. Farragi, V. Lyahovitskaya, and S. Vega, Phys. Rev. B **56**, 6712 (1997).
[18] A. Lewicki, A. I. Schindler, I. Miotkowski, and J. K. Furdyna, Phys. Rev. B **41**, 4653 (1990).
[19] N. Adachi, G. Kido, Y. Nakagawa, Y. Oka, and J. R. Anderson, J. Magn. Magn. Mater. **90&91**, 778 (1990).
[20] E. A. Turov and M. P. Petrov, *Nuclear Magnetic Resonance in Ferro- and Antiferromagnets* (Halsted, New York, 1972).
[21] J. Herzfeld, and A. E. Berger, J. Chem. Phys. **73**, 6021 (1980).
[22] J. P. Jesson, in *NMR of Paramagnetic Molecules*, edited by G. N. Lamar, W. Den Horrucks, Jr., and R. H. Holm (Academic, New York, 1973).
[23] I. Solomon, Phys. Rev. **99**, 559 (1955).